

## Supplementary Information

# Controllable Synthesis of Ultra-Small Metal-Organic Framework Nanocrystals Composed of Copper(II) Carboxylates

Xiangxing Xu\*

School of Chemistry and Materials Science, Nanjing Normal University, Nanjing 210046, P. R. China.

\*Correspondence to: xuxx@njnu.edu.cn

## 1. Experimental:

**Chemicals.** All reagents and solvents employed were commercially available and used as received without further purification. Ethanol (AR), cyclohexane (AR), N,N-dimethylformamide (DMF, AR), dimethyl sulfoxide (DMSO, AR), Sodium hydroxide (NaOH, AR), sodium oleate (CP), copper(II) nitrate trihydrate ( $\text{Cu}(\text{NO}_3)_2 \cdot 3\text{H}_2\text{O}$ , AR), iron(II) sulfate heptahydrate ( $\text{FeSO}_4 \cdot 7\text{H}_2\text{O}$ , AR), iron(III) nitrate nonahydrate ( $\text{Fe}(\text{NO}_3)_3 \cdot 9\text{H}_2\text{O}$ , AR), cobalt(II) nitrate hexahydrate ( $\text{Co}(\text{NO}_3)_2 \cdot 6\text{H}_2\text{O}$ , AR), nickel(II) nitrate hexahydrate ( $\text{Ni}(\text{NO}_3)_2 \cdot 6\text{H}_2\text{O}$ , AR), manganese(II) nitrate tetrahydrate ( $\text{Mn}(\text{NO}_3)_2 \cdot 4\text{H}_2\text{O}$ , AR), ruthenium(III) chloride hydrate ( $\text{RuCl}_3 \cdot x\text{H}_2\text{O}$ , 3N), hexanoic acid (CP), 4,4'-biphenyldicarboxylic acid (BPDCA, 98%), 1,4-benzenedicarboxylic acid (BDCA, 99%), benzene-1,3,5-tricarboxylic acid (BTCA, 98%), oleylamine (80–90%), n-hexylamine (99%) and n-octylamine (99%) were obtained from Sinopharm (SCRC). 1,3,5-tris(4-carboxyphenyl)benzene (TCPB or  $\text{H}_3\text{BTB}$ , >98%) was obtained from TCI. Dodecylamine (98+%) and oleic acid (tech. 90%) were purchased from Alfa Aesar. Octadecylamine (>99.0%, GC) and hexadecylamine (98%) were purchased from Sigma-Aldrich.

**Instruments.** The emulsion size of the reaction system was investigated by dynamic light scattering equipment BI-200SM (Brookhaven). The powder X-ray Diffraction (XRD) spectra were performed on a Bruker D8 Advance instrument with a Cu  $K\alpha$  radiation ( $\lambda = 1.5418 \text{ \AA}$ ). The inductively coupled plasma optical emission spectrometer (ICP-OES) measurement was

performed by Optima 5300DV (Perkin-Elmer Instruments). The UV-vis absorption spectra were measured by a Shimadzu UV-2700 UV-vis spectrophotometer. The Fourier transform infrared spectroscopy (FTIR) spectra were collected by a VECTOR 22 spectrometer with KBr pellets at a resolution of  $2\text{ cm}^{-1}$ . The transmission electron microscopy (TEM) images were obtained by employing a JEM-2100 TEM with the acceleration voltage of 200 kV and HT7700 (Hitachi) at 80 kV. The scanning electron microscopy (SEM) images were obtained on the S-4800 SEM at 20kV. The XPS spectrum was recorded by a PHI 5000 VersaProbe (U1VAC-PHI). The Atomic Force Microscopy (AFM) measurement was conducted on a Dimension FastScan Bio (Bruker). Thermogravimetric analysis and differential scanning calorimetry (TGA/DSC) was collected on a Perkin-Elmer Pyris 1 TGA analyzer. The metal ion exchange ratio was obtained by energy dispersive x-ray spectroscopy (EDS) equipped with the SEM. The I-V curves were measured by semiconductor device analyzer B1500A from Agilent Technologies.

**Metal-oleate precursors** were prepared by ion exchange with sodium oleate. Typically, sodium oleate (20 mmol) was dissolved in the mixture of 40 ml  $\text{H}_2\text{O}$  and 20 ml ethanol by sonication. Copper(II) nitrate solution (10 ml, 1 M) was quickly added in with stirring. A green precipitate was formed immediately. The supernatant was discarded and the waxy product was washed with  $\text{H}_2\text{O}$ -ethanol (v:v=1:1). The Cu(II)-oleate was dissolved in 100 ml cyclohexane, forming a transparent green solution (0.1 M). Minors of  $\text{H}_2\text{O}$  or insolubles in the solution was separated and removed by centrifugation (4000 rpm, 3min). Other metal-oleates (Fe(II/III)-oleate, Co(II)-oleate, Ni(II)-oleate, Mn(II), Ru(III)-oleate, Ag(I)-oleate, etc.) were prepared in a similar way. Cu(II)-caproate was prepared by the reaction of  $\text{Cu}(\text{OH})_2$  with hexanoic acid.

**Synthesis of HKUST-1.** A HKUST-1 precursor solution was prepared by dissolving  $\text{Cu}(\text{NO}_3)_2 \cdot 3\text{H}_2\text{O}$  (61 mg) and 1,3,5-benzenetricarboxylic acid (30 mg) in DMSO (0.5 ml). Powder samples are obtained by evaporating this solution at 373 K. The resulting HKUST-1 was washed with ethanol and dried at 400 K.

**Synthesis of Cu-BTC MOF nanocrystal (sample S18-3).** In a typical synthesis of  $\sim 2\text{ nm}$  Cu-BTC MOF (known as HKUST-1 with the molecular formula  $\text{Cu}_3(\text{BTC})_2$ ), oleylamine (0.35 mmol) was added to 4 ml cyclohexane solution of Cu(II)-oleate (0.1 mmol), forming a deep blue solution. 1,3,5-Benzenetricarboxylic acid (BTCA, 10 mg, 0.047 mmol) in dimethyl sulphoxide (DMSO, 0.1 ml) and ethanol (0.4 ml) mixture solution was injected in with vigorous stirring at room temperature ( $\sim 20\text{ }^\circ\text{C}$ ) for 30 min. The as synthesized products was precipitated by adding 4

ml ethanol and gathered by centrifugation (14000 rpm, 1 min), yielding ~20 mg MOF nanocrystals. The solid product redispersed well in nonpolar solvent such as cyclohexane or toluene, forming a transparent blue solution.

**Size control of the Cu-BTC MOF nanocrystals.** In control experiments studying the oleylamine coordination effect, oleylamine of 0, 0.15, 0.25, 0.35 and 0.7 mmol was used with other parameters the same as above; In studying the alkyl chain length of the amine ligand, the amine was fixed 0.35 mmol with other parameters the same; In studying the alkyl chain length of carboxylic ligand, Cu(II)-caproate 0.1 mmol was used with else parameters the same.

**Multi-injection synthesis of Cu-BTC MOF nanocrystals.** Precursors for the multi-injection were prepared as that was used for the Cu-BTC MOF nanocrystal synthesis. Specifically, precursor A was formed by mixing oleylamine (0.7 mmol) with Cu(II)-oleate (0.2 mmol) in 5 ml cyclohexane; Precursor B was made by dissolving *BTCA* (21 mg) in the mixture of DMSO (0.2 ml), ethanol (0.8 ml) and cyclohexane (1 ml). Precursor B and precursor A were alternatively added in to the Cu-MOF nanocrystal cyclohexane solution (~22 mg in 2 ml) with vigorous stirring. The time interval for each injection was 5 min. In each injection, 125  $\mu$ l precursor A or 50  $\mu$ l precursor B was introduced, respectively.

**Self-assembly of Cu-BTC MOF nanocrystals.** In studying the self-assembly mechanism of Cu-BTC MOF cubes, the reaction system was the same as the above to synthesize S18-3 MOF nanocrystals. The reaction solution was enclosed in a Teflon lined autoclave and put in the heating oven with the temperature setting at 40 or 60 °C and time setting 8 hrs. The product was collected at the bottom of the autoclave for the 60 °C sample; For the 40 °C sample, the product was collected by ethanol precipitation and centrifugation. In studying the self-assembly of 2D MOF nano flakes, the reaction system was exactly the same as the 2 nm Cu-BTC MOF synthesis, except the reaction time prolonged for 2 days. The final reaction solution was a little turbid. It was centrifuged directly without adding ethanol (14000 rpm, 1 min). The minor precipitate is the assembled MOF flakes. The major production is unassembled MOF nanocrystals of ~2 nm which can be separated from the supernatant by adding ethanol and centrifugation.

**Synthesis of Cu-BDC MOF nanocrystals.** Solution A was prepared by adding oleylamine (60 mg) to 4 ml cyclohexane solution of Cu(II)-oleate (0.1 mmol). Solution B was prepared by dissolving *BDCA* (8.3 mg, 0.05 mmol) in the mixture of DMF (0.2 ml) and ethanol (0.3 ml).

Solution B was injected into solution A with magnetic stirring for 10 min. Ethanol was added to precipitate the Cu-BDC MOF nanocrystals followed by centrifugation.

**Synthesis of Cu-BPDC MOF nanocrystals.** BPDCA (10 mg, 0.041 mmol) was dissolved in DMF (4 ml) forming solution A. Solution B was prepared by adding oleylamine (90 mg) to 4.5 ml cyclohexane solution of Cu(II)-oleate (0.2 mmol). With vigorous stirring, 1 ml of solution A was added into solution B and let reaction for 30 min. The reaction solution was centrifuged (14000 rpm, 30 sec). The supernatant was taken out, adding 5 ml of ethanol, followed by purifying again by centrifugation. The supernatant was taken out, adding 1 ml of solution A. Precipitate was formed instantly and the product was collected by centrifugation. The as synthesized Cu-BPDC MOF nanocrystals are well redispersed in nonpolar solvent, forming a clear blue solution.

**Synthesis of Cu-TCPB MOF nanocrystals.** Typically, oleylamine (45 mg) was added to 4 ml cyclohexane solution of Cu(II)-oleate (0.1 mmol) as solution A. TCPB (7.5 mg, 0.017 mmol) was dissolved in the mixture of DMSO (0.2 ml) and ethanol (0.8 ml). It was injected into solution A for reaction with stirring for 10 min. Ethanol (3 ml) was add and centrifuged to separate the MOF nanocrystals.

**Ion exchange.** Cyclohexane solution (0.1 M) of metal-oleate (Fe(II/III), Co(II), Ni(II), Mn(II), Ru(III), etc.) was used as the ion exchange agents. It was mixed with the Cu-BTC MOF nanocrystals in cyclohexane for 5 minutes, followed by adding ethanol to precipitate the product, separated by centrifugation (14000 rpm, 1 min). Redispersed in cyclohexane, it was washed by ethanol, centrifuged again to eliminate residual metal-oleates which remained in the supernatant. The exchange ratio is controlled by the amount of the metal-oleates used.

**Film spin-coating.** Cyclohexane solution of Cu-BTC MOF nanocrystals with the concentration of ~22 mg/ml was adopted as the spin-coating source. Typically, 6–8 droplets of the solution were transferred on to a quartz slide, covering the whole 15×15 square. Followed by accelerating to 2600 rpm in seconds, the speed was sustained for 30 seconds. This spin-coating can be repeated for many times as needed. We denote ‘×1’ for spin-coating once and ‘×n’ for a multi spin-coating for totally n times. A ‘×1’ sample was scratched by a syringe needle head to expose the quartz substrate. The edge of the scratch was characterized by AFM, from which the thickness was revealed. Using this data, the thickness of ‘×n’ films was also extracted from the transmission spectra of the films.

**Thermal treatment.** The spin-coated ‘×n’ films were thermal treated either in air in a muffle furnace or in a tubular furnace with Ar protection at certain temperatures (200, 260, 320 or 450 °C) for 10 min, followed by natural cooling.

**Equations.** The weight of a colloidal nanocrystal ( $W_{NC}$ ) contains two fractions, the weights of bare nanocrystal core and the ligands:

$$W_{NC} = W_{core} + W_{ligands} \quad (1)$$

Given the core has a constant density ( $\rho_{core}$ ), its weight is proportional to the volume, written as:

$$W_{core} = \rho_{core} V_{core} = A_1 \rho_{core} R_{eff}^3 \quad (2)$$

Where  $A_1$  is a shape related parameter and  $R_{eff}$  is the effective radius. The weight of ligands on a nanocrystal is given by:

$$W_{ligands} = \rho_{surf} S_{core} = A_2 \rho_{surf} R_{eff}^2 \quad (3)$$

Where  $A_2$  is a shape related parameter and  $\rho_{surf}$  is the surface density of the ligands on the nanocrystal surface. The surface density  $\rho_{surf}$  would vary with different surface ligands because of the steric effect difference. The weight ratio of the ligands to core is:

$$S = \frac{W_{ligands}}{W_{core}} = \frac{A_2 \rho_{surf}}{A_1 \rho_{core}} \times \frac{1}{R_{eff}} \quad (4)$$

From equation (1–3), the total weight of the MOF nanocrystals can be expressed as:

$$W = \sum_n W_{NC} = Y\% \times \left( A + B \times \frac{1}{R_{eff}} \right) \quad (5)$$

Where  $n$  is the number of the nanocrystals;  $Y\%$  is production yield of the nanocrystal core;  $A$  and  $B$  are constants that functional to  $\rho_{core}$ ,  $\rho_{surf}$  and shape factor.

## 2. Figures and Tables:

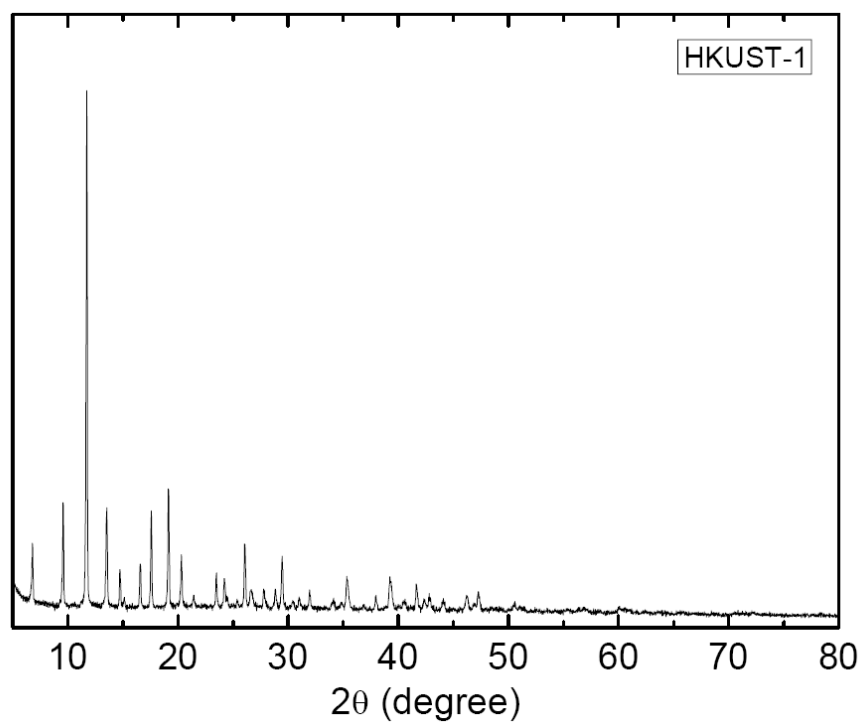


**Figure S1.** XRD spectrum of the MOF material synthesized by a reported method [Ref. S1]. It matches well with the HKUST-1 structure and no impurity such as Cu, Cu<sub>2</sub>O, CuO or Cu(OH)<sub>2</sub> was detected from the XRD spectrum.

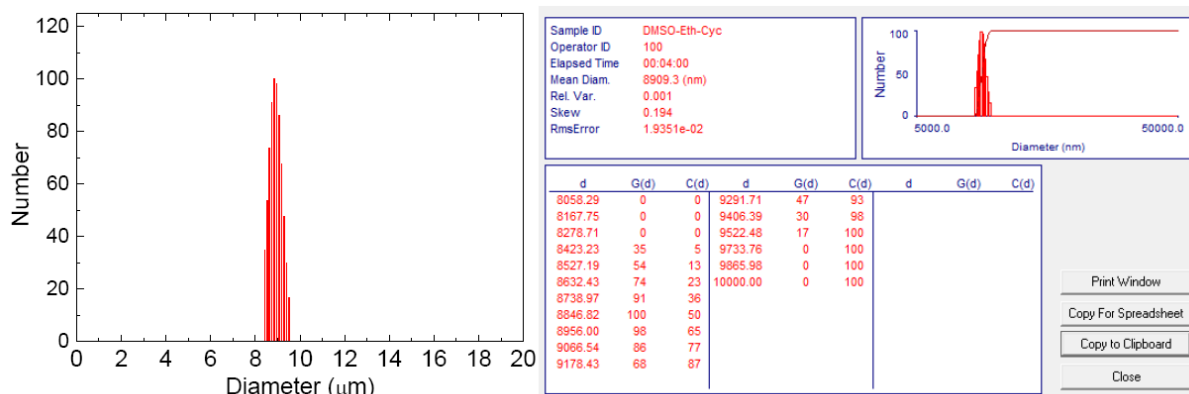


**Figure S2.** Dynamic light scattering measurement of the reaction solution system (without BTC linkers) in synthesizing sample S18-3: cyclohexane (4 ml), oleylamine (90 mg), Cu-oleate (0.1 mmol), DMSO (0.1 ml) and ethanol (0.4 ml) at room temperature (20 °C). It suggests that the DMSO is of the emulsion form in the solution with a narrow size distribution of about 9  $\mu\text{m}$ .

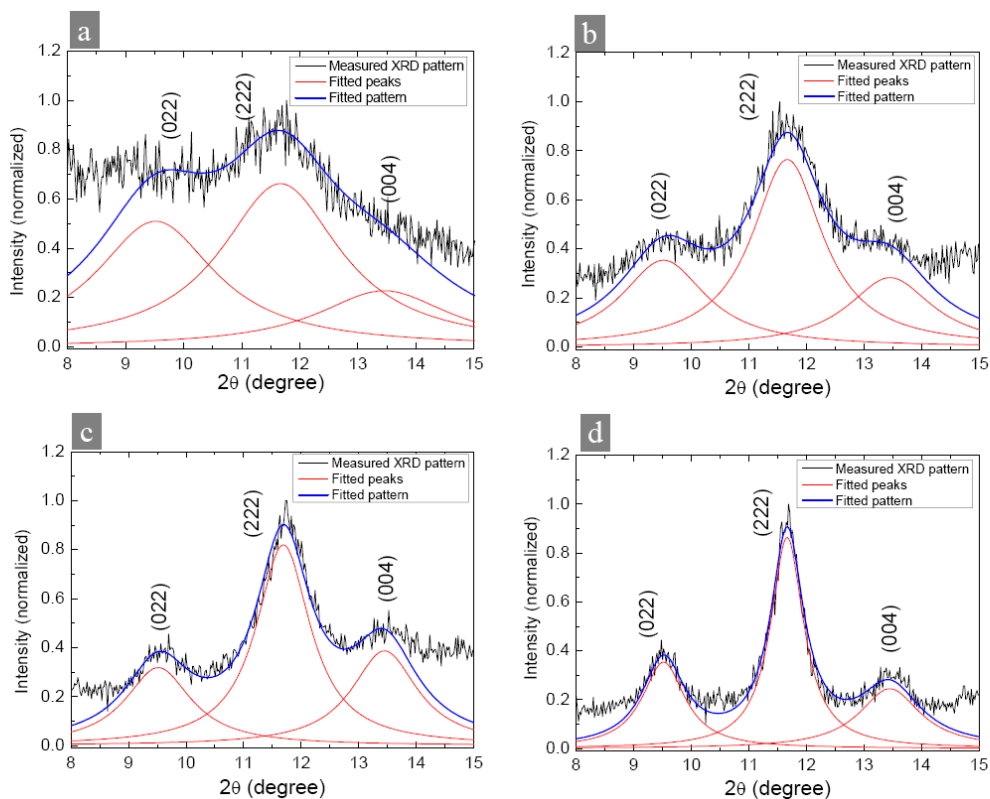


Figure S3. The fitting of XRD patterns of Cu-BTC MOF nanocrystals. The size of Cu-BTC MOF nanocrystals was also estimated by Scherrer equation from the XRD pattern:

$$D = \frac{K\lambda}{\beta \cos(\theta)}$$

where  $D$  is the nanocrystal size;  $K$  is a constant;  $\lambda$  is the X-ray wavelength of 0.154 nm;  $\theta$  is the Bragg angle of the peak. Take  $K=1$  when using integration width (IW) of the peak as  $\beta$ ;  $K=0.89$  when using full width at high maximum (FWHM) of the peak as  $\beta$ . The value of  $\beta$  is extracted by using Lorentzian fitting (See (a), (b), (c) and (d) above, for sample M-2, C18-1, C18-3 and C12, respectively). In this investigation, the nanocrystal size is estimated by the average value from the fitted (022), (222) and (004) peaks, which are strong and less overlapped with adjacent peaks. The TEM/HRTEM measured average diameters of ~1.2, 1.5, 2.0 and 2.5 nm are corresponding to the values of 2.2, 3.3, 4.3 and 6.2 nm calculated by Scherrer equation (Table S1). This discrepancy may result from three facts. First, Scherrer equation is semi-quantitative. Second, the contrast of the outer layer of these ultra small MOF nanocrystals is too low to be clearly identified by TEM/HRTEM, just as the organic ligands layer on nanocrystals can not be clearly characterized by TEM/HRTEM in most reported cases. Third, the size distribution contributes differently in these two size estimation methods. For the MOF nanocrystal diameter measured by TEM/HRTEM is visible for statistic count and likely approaching the inner core size of the MOF nanocrystals, it is used for discussion in this paper.

**Table S1.** Average size of the Cu-BTC MOF nanocrystals estimated from TEM and XRD.

Sample	TEM measured average size (nm)	Scherrer equation estimated average size using $IW \beta$ (nm)	Scherrer equation estimated average size using FWHM $\beta$ (nm)
M-2	~1.2	2.2	3.0
C18-1	1.5	3.3	4.7
C18-3	2.0	4.3	6.1
C12	2.5	6.2	8.7

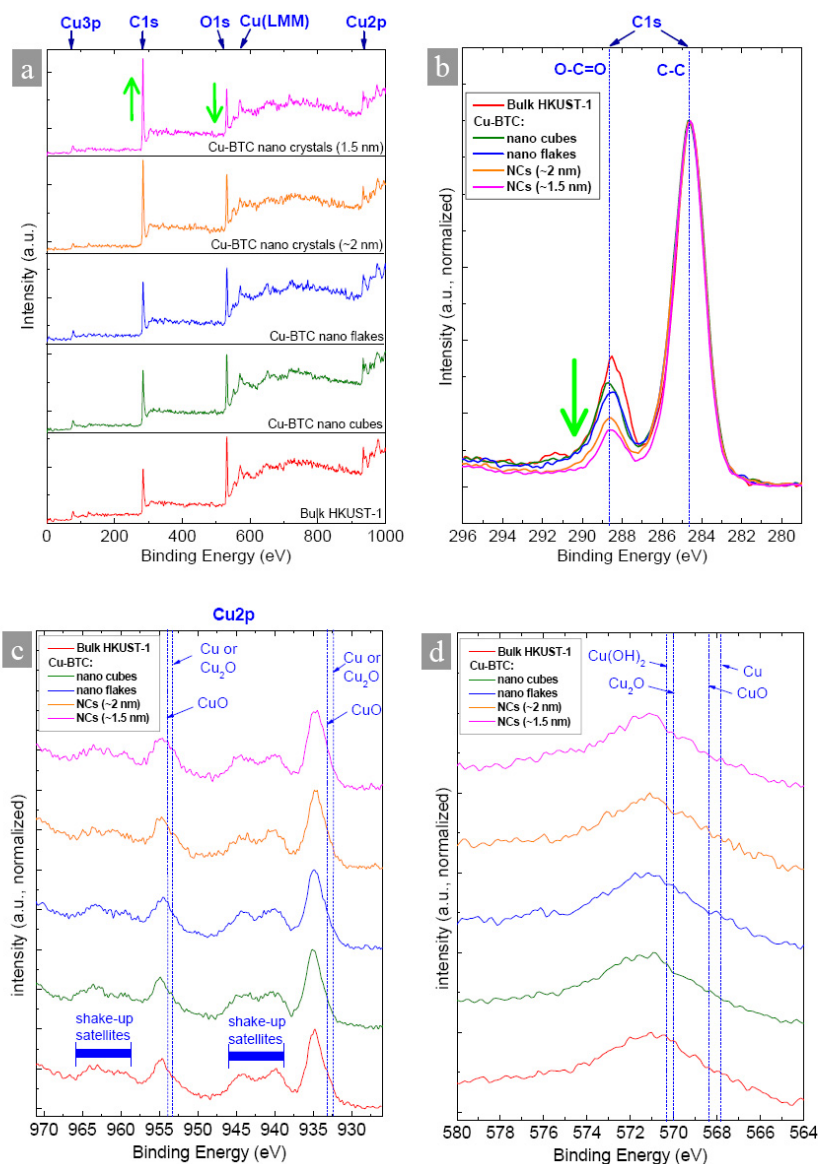


**Figure S4.** XPS spectra of Cu-BTC MOF nanocrystals, nano flakes, nano cubes, and reference HKUST-1 sample. (a) binding energy of Cu 2p, (b) Cu LMM Auger transition, (c) C 1s and (d) survey scan spectrum. The XPS spectra reveal higher intensity ratios of C1s to O1s and C1s<sub>(C-C)</sub> to C1s<sub>(O-C=O)</sub> of smaller Cu-BTC nanocrystals compared with those of the larger and the reference HKUST-1 sample, suggesting the presence of coordinated surface ligands of oleate and/or oleylamine which has long alkyl group. The Cu 2p<sub>3/2</sub> and Cu 2p<sub>1/2</sub> peaks respectively locate at 935.1 and 954.8 eV, apart from the corresponding peaks of Cu(0) or Cu(I) in the form of Cu or Cu<sub>2</sub>O at 932.4 and 953.1 eV; the presence of the “shake-up satellites” around 942 and 964 eV is characteristic of an open 3d<sup>9</sup> shell, corresponding to Cu(II) state. The Cu LMM Auger peak at 571.3 eV deviates from that of the Cu and CuO, at 567.8 and 568.3 eV, respectively. [Ref. S2–S5]

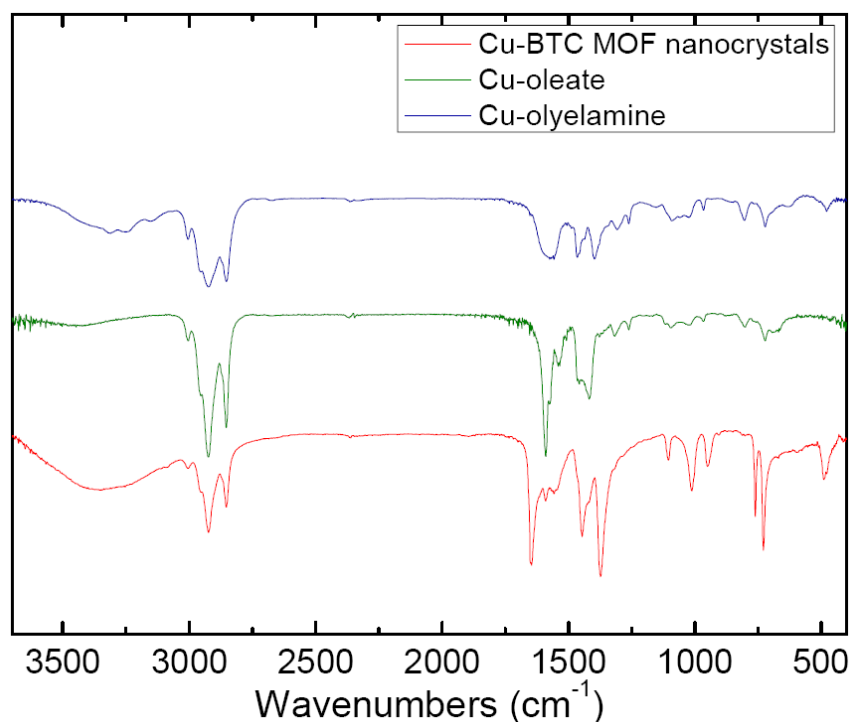


**Figure S5.** The Fourier transform infrared (FTIR) spectra of the precursor species (Cu-oleate and Cu-oleylamine) and the Cu-BTC MOF nanocrystals. The FTIR spectrum of the Cu-BTC MOF nanocrystals is in good agreement with the published data of HKUST-1 in the 400–2500  $\text{cm}^{-1}$  range [Ref. S6–S8]. The peaks at 1646, 1590  $\text{cm}^{-1}$  and 1446, 1373  $\text{cm}^{-1}$  corresponded to asymmetric and symmetric vibration of coordinated carboxyl groups, respectively. The bands within 600–1200  $\text{cm}^{-1}$  are fingerprints associated with modes of the benzene ring. The 490  $\text{cm}^{-1}$  peak is the typical vibration mode directly involving Cu(II) species. The additional strong peaks at 2853 and 2924  $\text{cm}^{-1}$  are the  $\text{CH}_2$  symmetric and asymmetric stretching vibrations respectively, suggesting the presence of coordinated oleate and/or oleylamine as surface ligands.

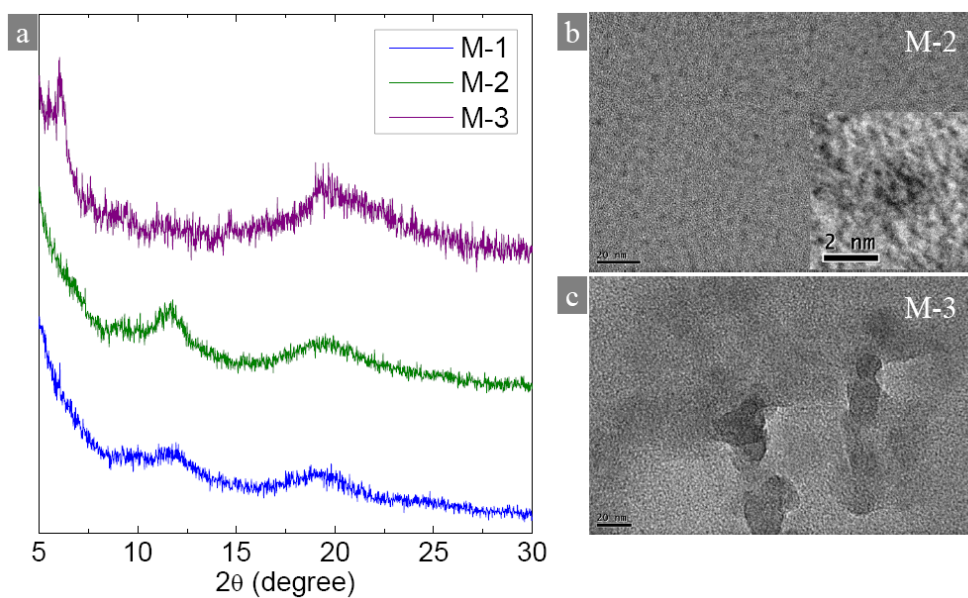


**Figure S6.** XRD and TEM/HRTEM measurement of Cu-BTC samples. (a) XRD patterns of Cu-BTC synthesized without oleylamine (M-1), with 0.12 mmol oleylamine (M-2) and with 0.45 mmol oleylamine (M-3). The M-1 sample is insoluble in cyclohexane. TEM/HRTEM images show that the M-2 sample contains ultra small nanoparticles in size of  $\sim 1\text{--}1.5$  nm (b), and amorphous colloidal without any shape for M-3 sample (c).

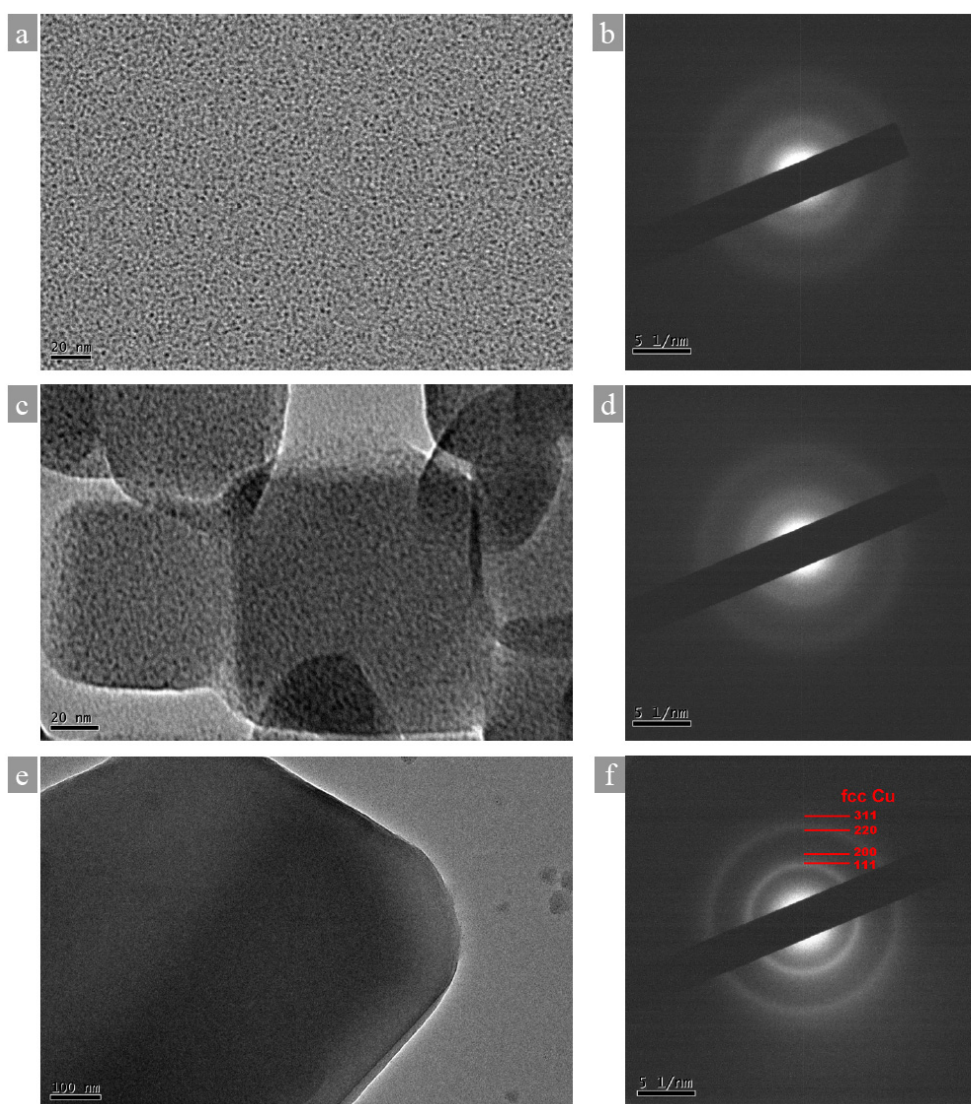


**Figure S7.** TEM and SAED characterization. (a) TEM image of multi layers of Cu-BTC nanocrystals and (b) corresponding SAED pattern. (c) TEM image of Cu-BTC nano cubes and (d) corresponding SAED pattern. (e) TEM image of a big HKUST-1 particle of the reference sample, and (f) corresponding SAED pattern. The SAED diffraction rings do not match that of the fcc structured copper, marked in red in (f). They do not match that of the  $\text{Cu}_2\text{O}$ ,  $\text{CuO}$  or  $\text{Cu}(\text{OH})_2$ , either. Therefore, the SAED patterns of these three samples are corresponding to the same structure of HKUST-1.

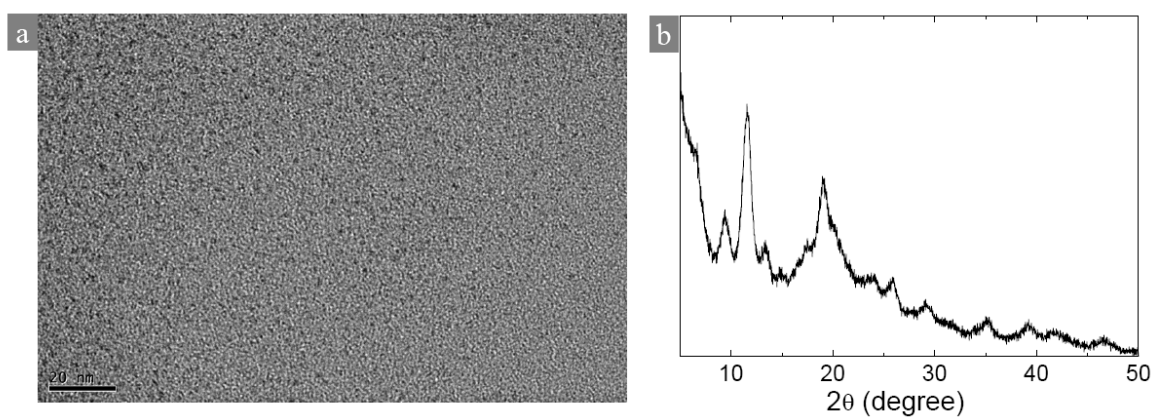


**Figure S8.** TEM and XRD characterization. TEM image (a) and XRD pattern (b) of Cu-BTC MOF nanocrystals synthesized with 0.5 mmol oleylamine and 0.6 mmol oleic acid.

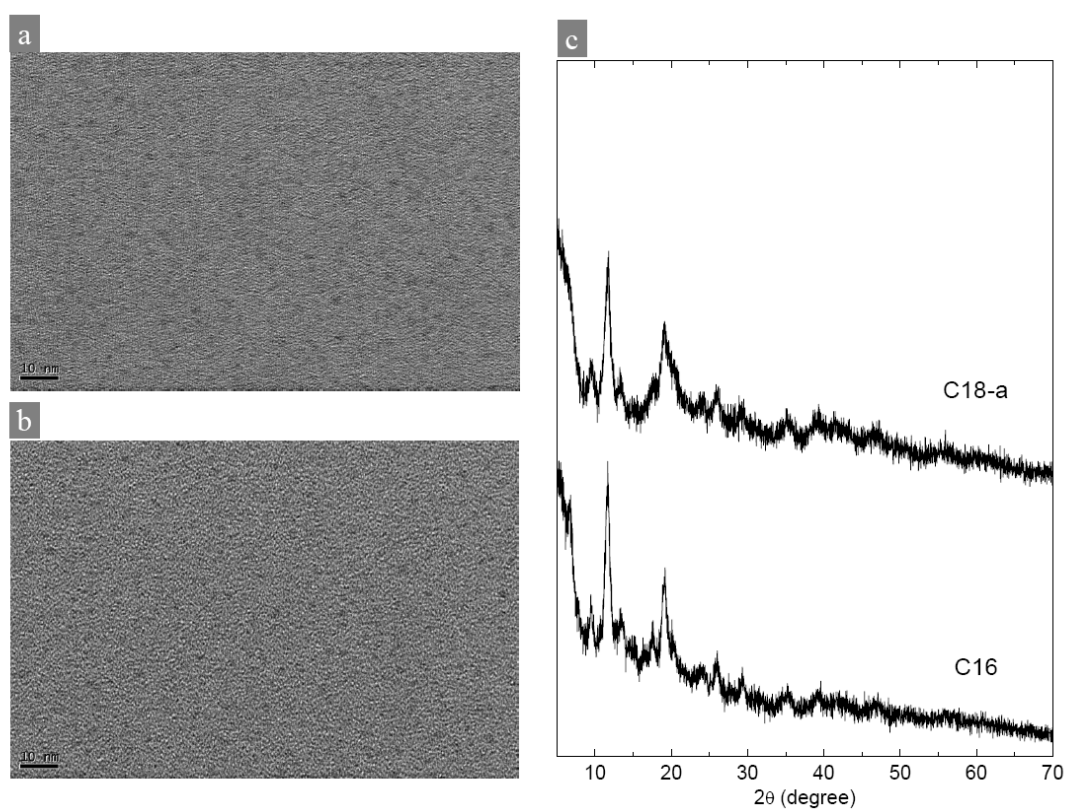


**Figure S9.** TEM and XRD characterization. TEM images of Cu-BTC MOF nanocrystals synthesized by (a) using hexadecylamine: C16 (~2 nm) and (b) octadecylamine: C18-a (~2 nm). (c) Corresponding XRD patterns.

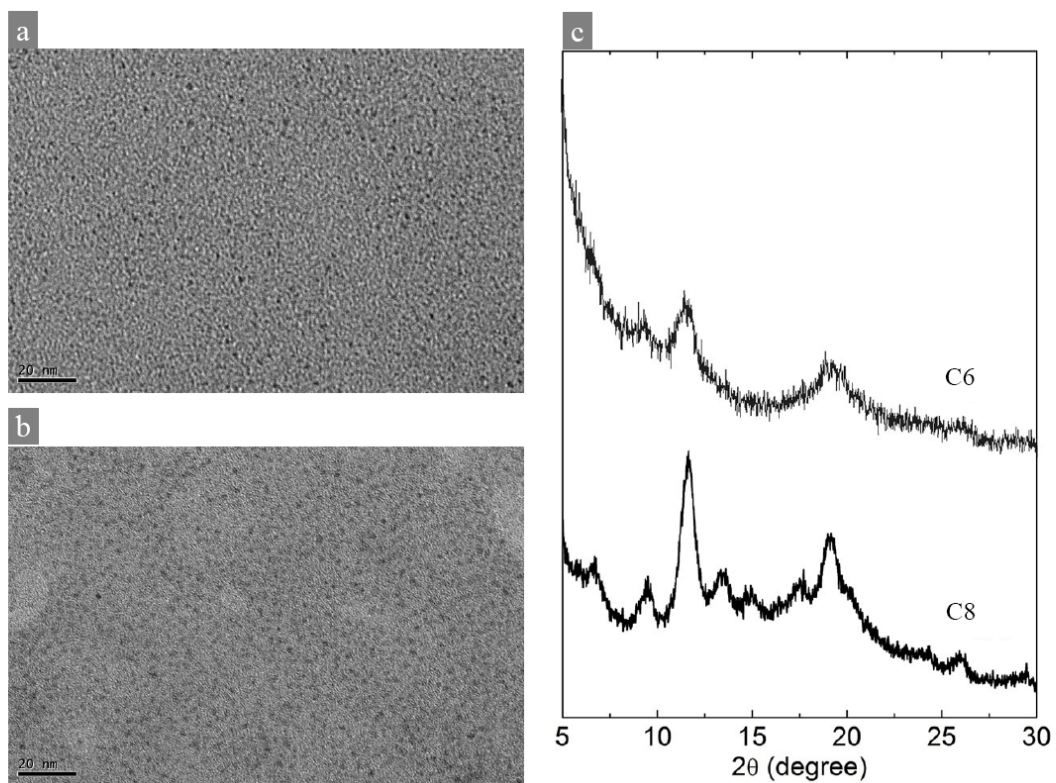


**Figure S10.** TEM and XRD characterization. TEM/HRTEM images of Cu-BTC MOF nanocrystals synthesized by (a) using 1-hexylamine: C6 (~1.5 nm) and (b) 1-octylamine: C8 (~2 nm). (c) Corresponding XRD patterns.

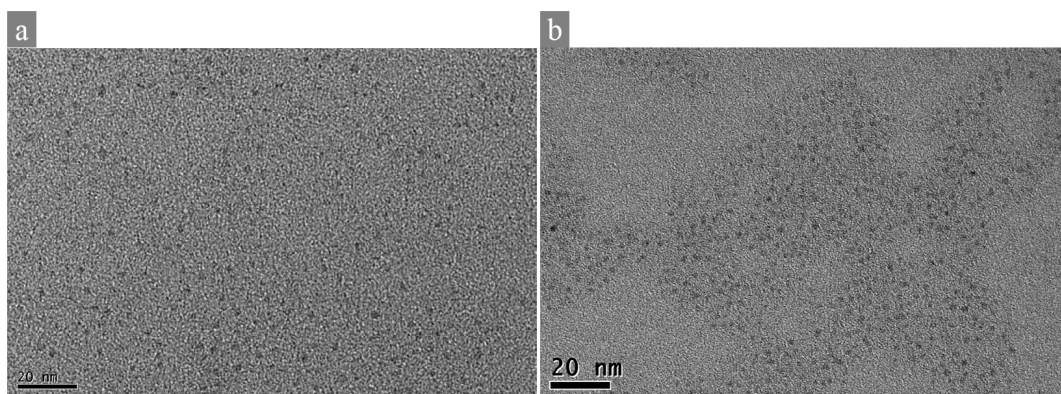


**Figure S11.** TEM images of Cu-BTC MOF nanocrystals. Cu-BTC MOF nanocrystals synthesized by mono-injection strategy (**a**), and by multi-injection strategy (**b**). No difference of the nanocrystal size ( $\sim 2$  nm) can be found of these two samples.

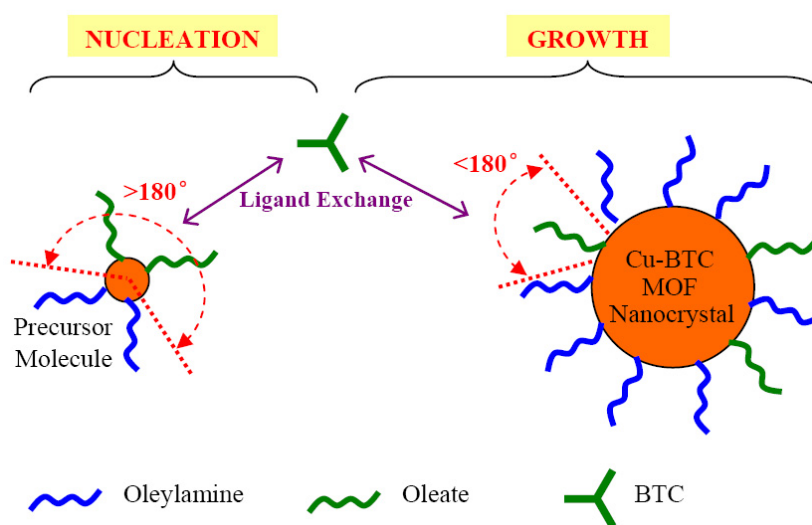


**Figure S12.** A schematic illustration of the different steric effect for the nucleation and growth of MOF nanocrystals. The Cu(II) precursors — Cu(II) oleate with ligands partially displaced by oleylamine ( $\text{Cu(II)(oleate)}_x(\text{oleylamine})_y$ ) — give ample space for BTC to approach the Cu(II) centre, while after the MOF nanocrystals are formed, additional steric effects induced by the MOF core hinders the growth. The stereo angle for the ligands exchange decreases as the MOF nanocrystal forms.

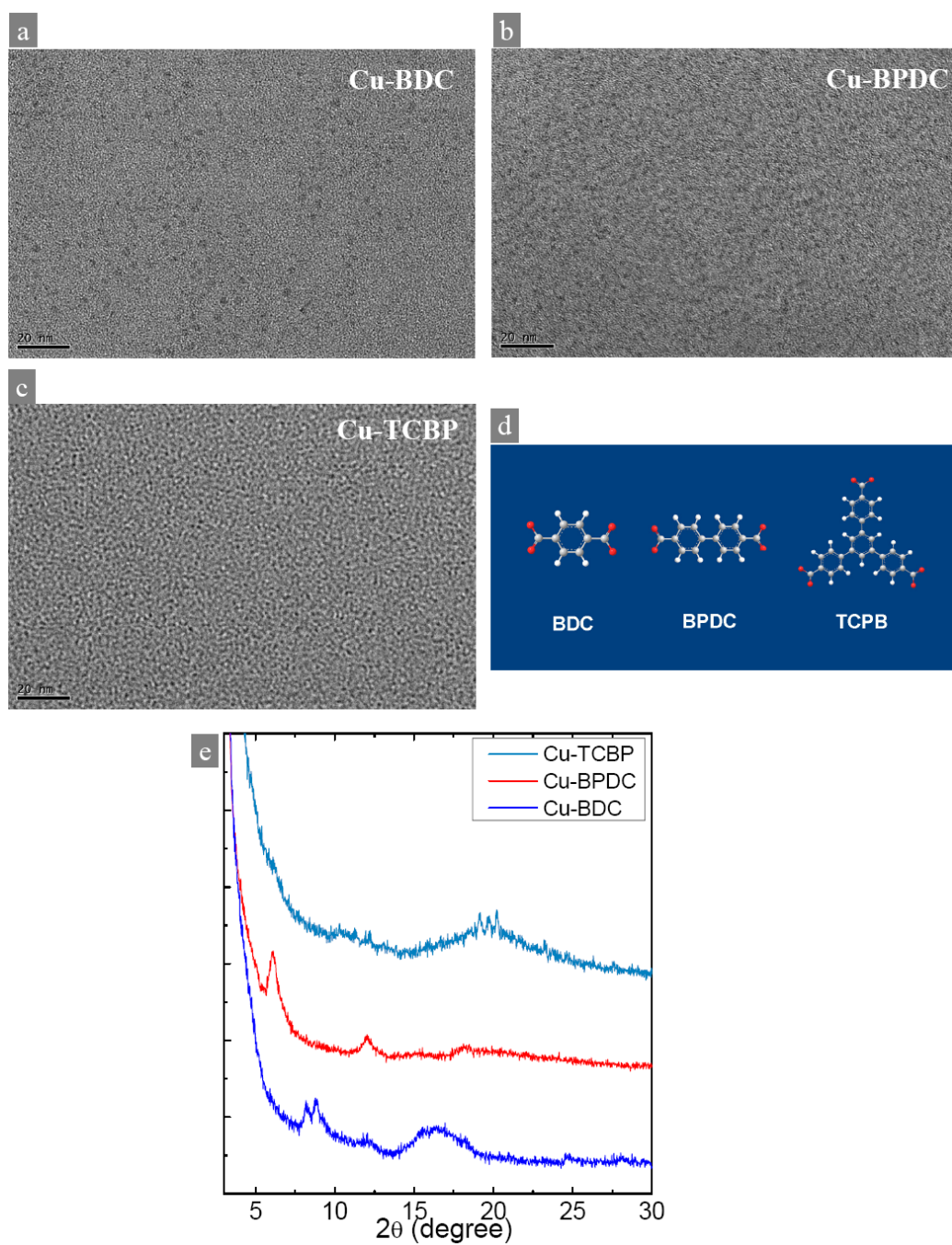


**Figure S13.** TEM and XRD characterization. (a–c) TEM images of Cu-BDC, Cu-BPDC and Cu-TCPB MOF nanocrystals, respectively. (d) The linking ligands. (e) XRD patterns. (scale bar for (a–c): 20 nm)

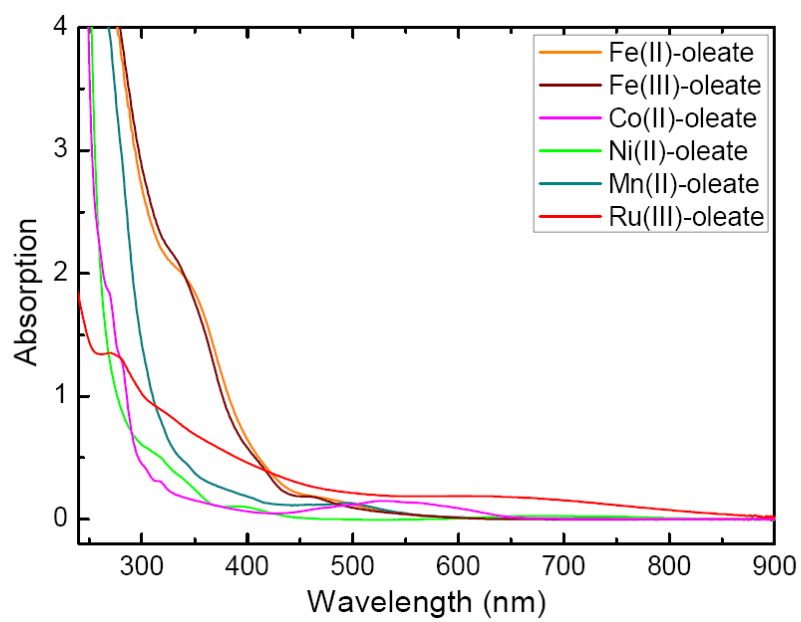


**Figure S14.** UV-vis spectra of the metal-oleates in cyclohexane solutions.

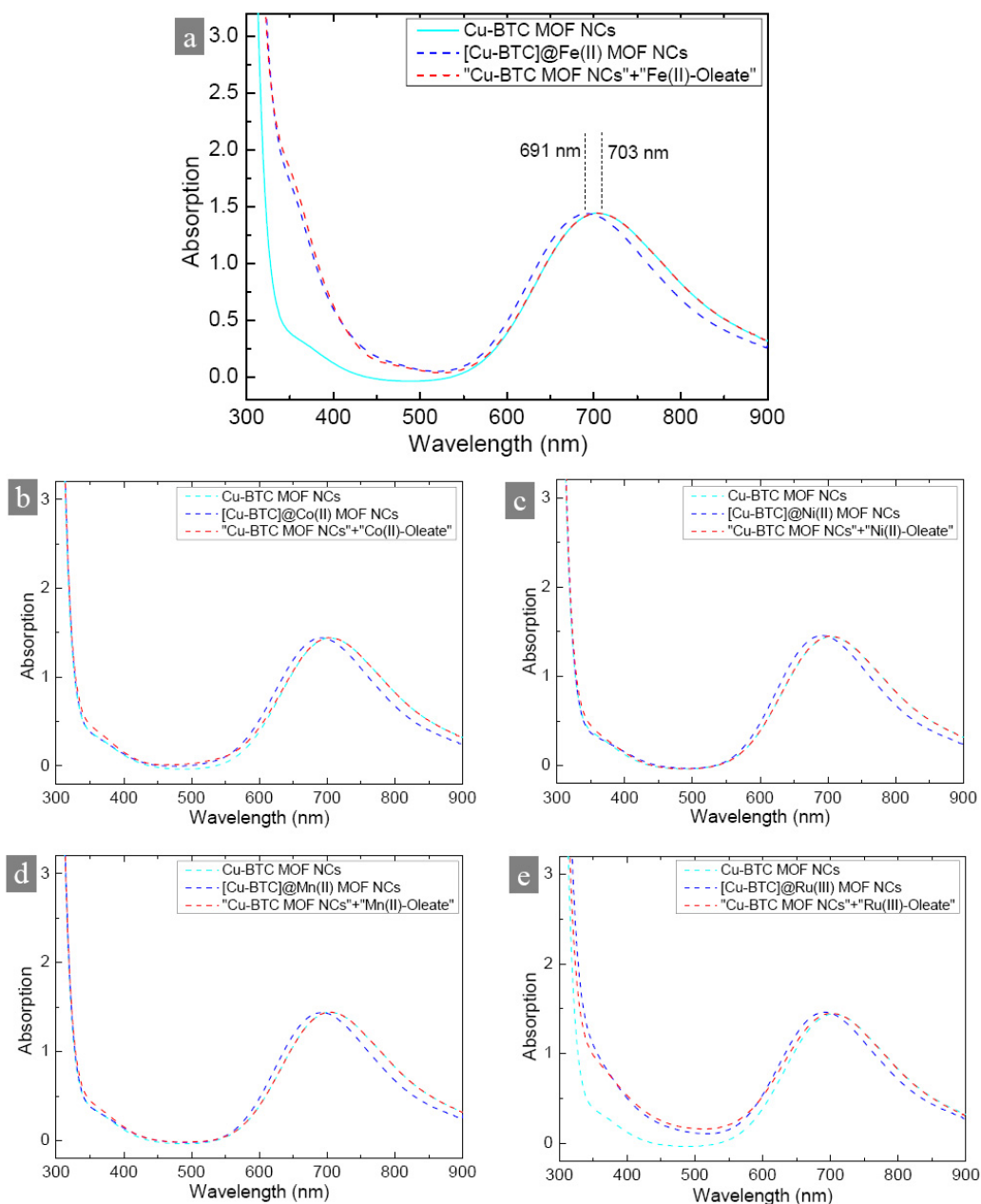


**Figure S15.** UV-vis spectra of the Cu-BTC MOF nanocrystals (Cyan dashed line), surface metal ion doped Cu-BTC MOF nanocrystals (blue dashed line), and spectra composed by Cu-BTC MOF nanocrystals and corresponding doping metal-oleates (red dashed line). By comparing the UV-vis spectra of these surface metal-ion doped MOF nanocrystals with the spectra composed by those of Cu-BTC MOF nanocrystals and corresponding metal-oleates, it can be found that they overlap within 300–550 nm range; while in the 550–900 nm realm, blue shift can be observed for all the surface metal ion doped Cu-BTC MOF nanocrystals compared with the un-doped Cu-BTC MOF nanocrystals, and the composed spectra share overlapped curves with that of un-doped nanocrystals. It may suggest a similar modulation of the Cu(II) coordination field in all these doped MOF nanocrystals.

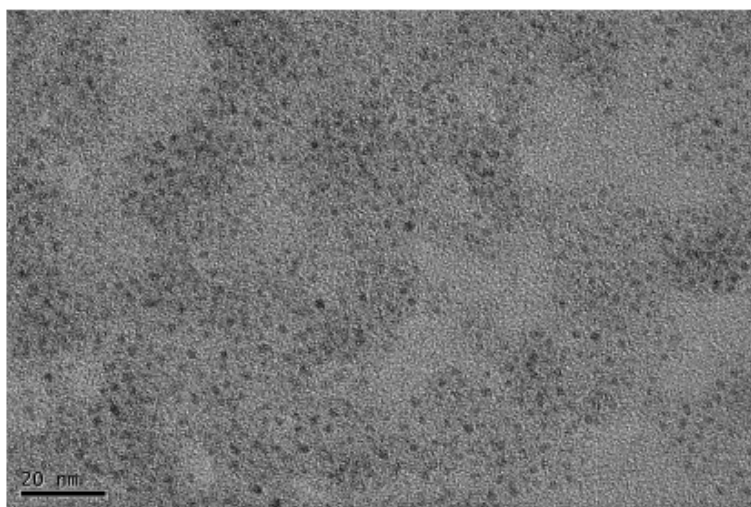


**Figure S16.** TEM image of the [Cu-BTC]@Fe(II) MOF nanocrystals (18.5%). (scale bar 20 nm)

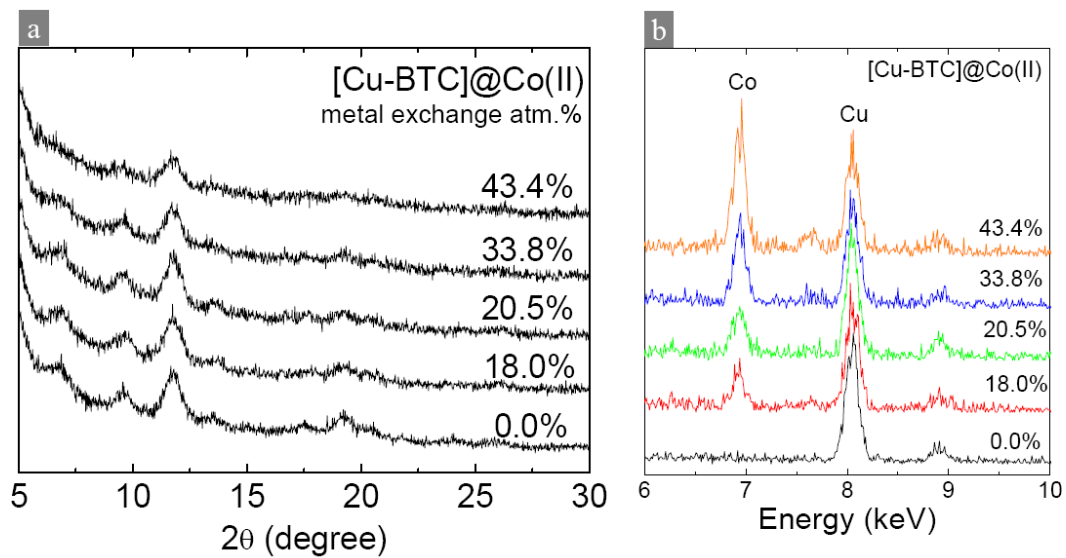


**Figure S17.** XRD and EDS characterization. (a) XRD patterns and (b) EDS spectra of the [Cu-BTC]@Co(II) MOF nanocrystals with doping level of 0–43.4%.

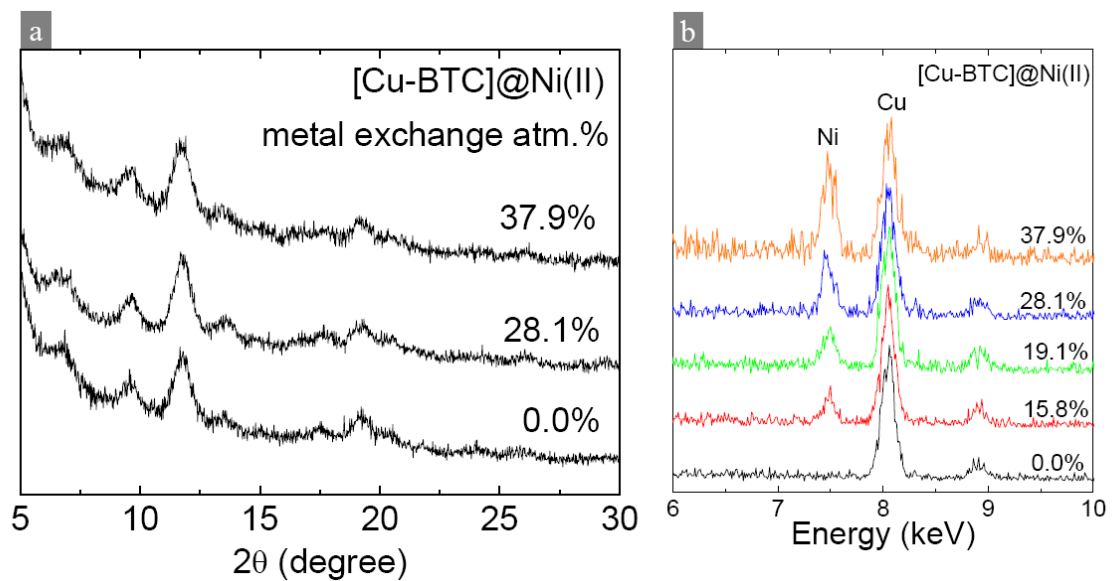


**Figure S18.** XRD and EDS characterization. (a) XRD patterns and (b) EDS spectra of the [Cu-BTC]@Ni(II) MOF nanocrystals with doping level of 0–37.9%.

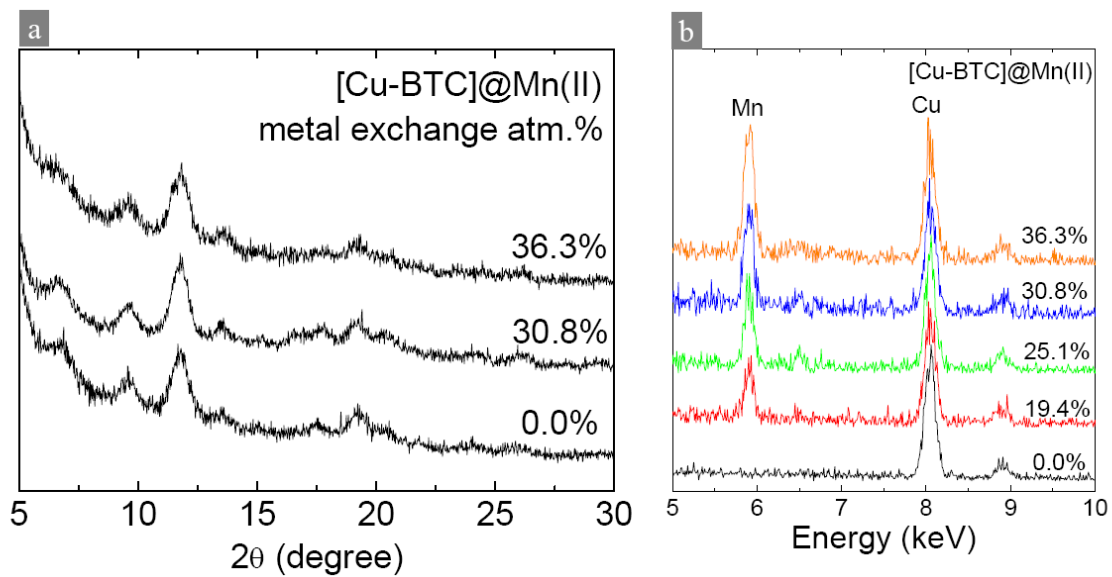


**Figure S19.** XRD and EDS characterization. (a) XRD patterns and (b) EDS spectra of the [Cu-BTC]@Mn(II) MOF nanocrystals with doping level of 0–36.3%.

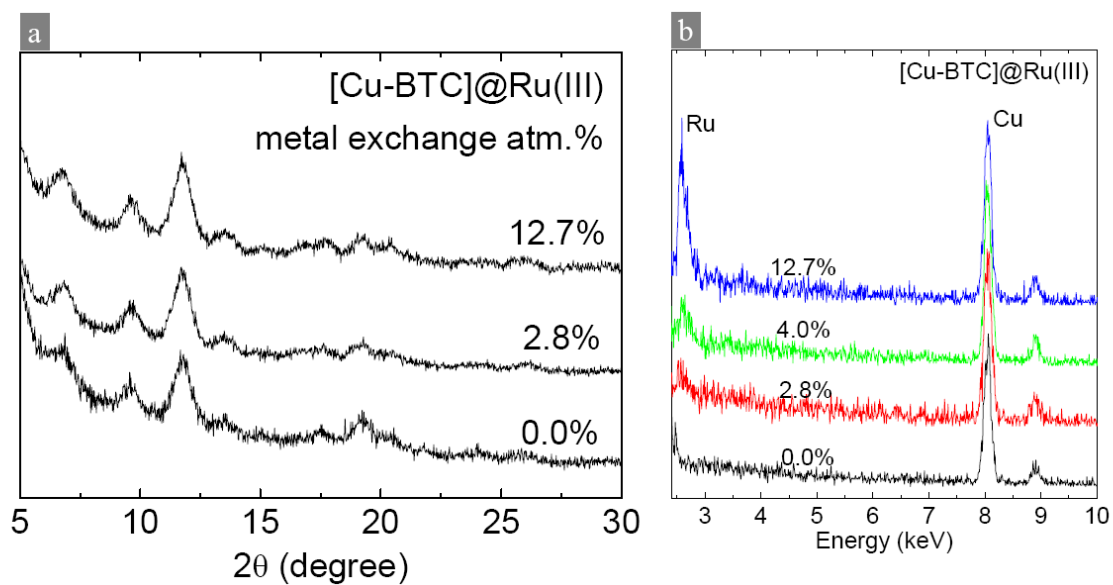


**Figure S20.** XRD and EDS characterization. (A) XRD patterns and (B) EDS spectra of the [Cu-BTC]@Ru(III) MOF nanocrystals with doping level of 0–12.7%.

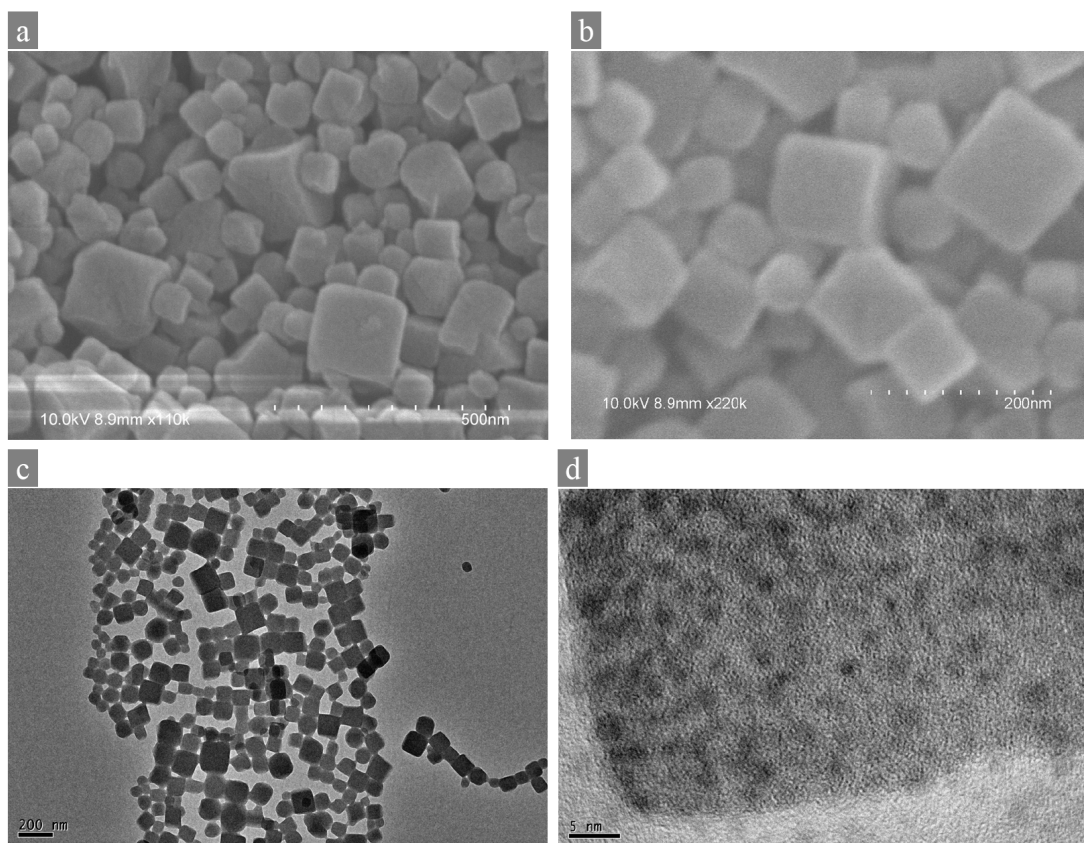


**Figure S21.** SEM and TEM/HRTEM characterization. (a) and (b) SEM images of 3D cubes self-assembled by Cu-BTC MOF nanocrystals. (c) and (d) the TEM/HRTEM images. (scale bar: (a) 500 nm, (b) 200 nm; (c) 200 nm and (d) 5 nm)

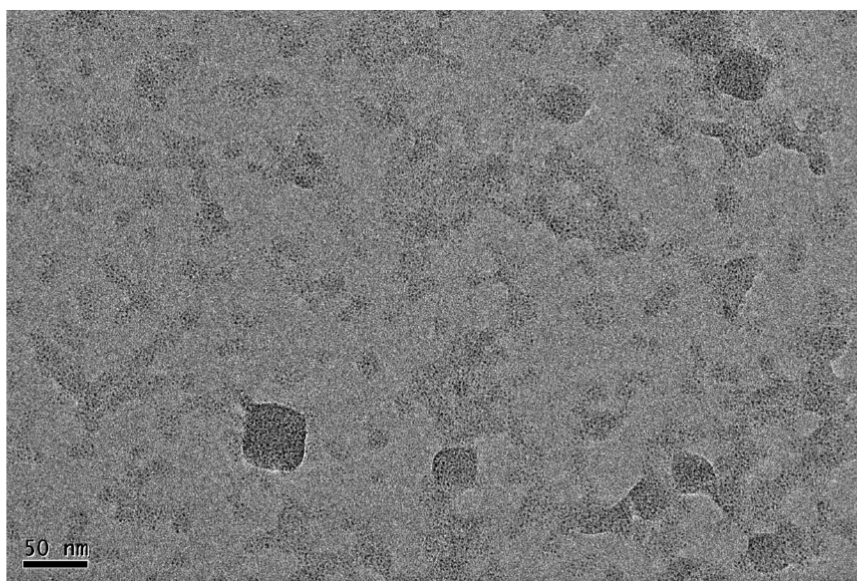


**Figure S22.** TEM image of Cu-BTC MOFs synthesized at 40 °C. It can be seen that the small Cu-BTC nanocrystals are on assembling of Cu-BTC MOF cubes.

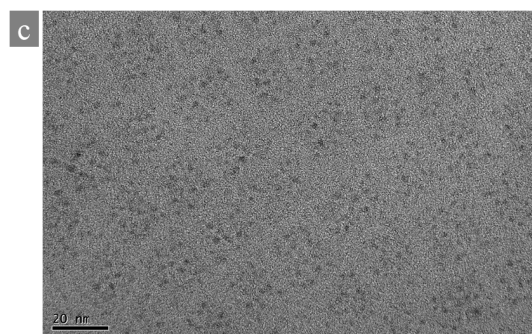
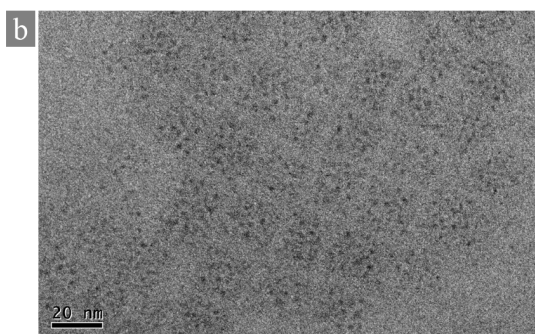
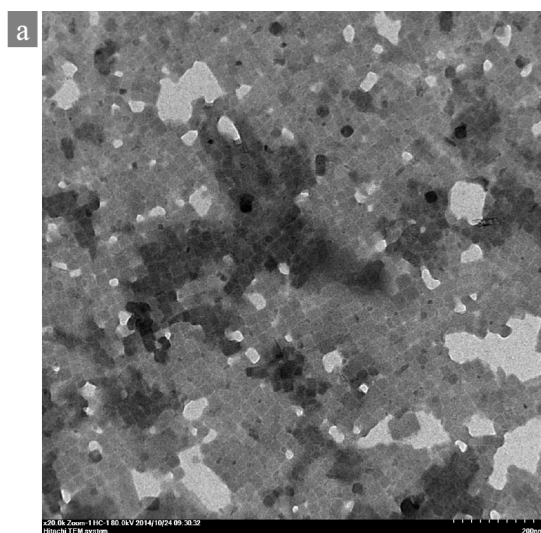


**Figure S23.** TEM images of 2D flakes self-assembled by Cu-BTC MOF nanocrystals. These examples in Fig. S25-27 indicate that despite of the structure featured in centre ion and organic linkers, MOF nanocrystals are same building blocks as other inorganic nanocrystals for higher scale level self-assembling structures [Ref. S9, S10]. (scale bar: (a) 200 nm (b,c) 20 nm; (a) is TEM image taken by HT7700 at 80 kV.)

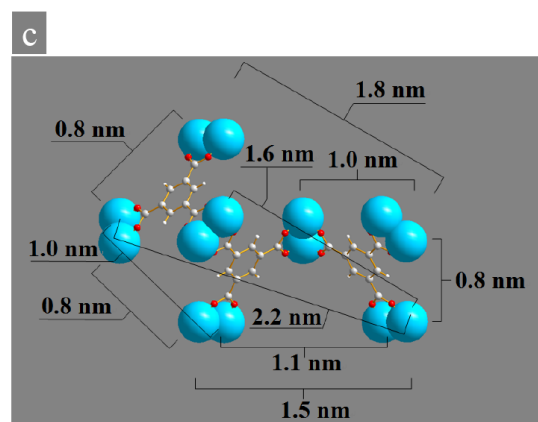
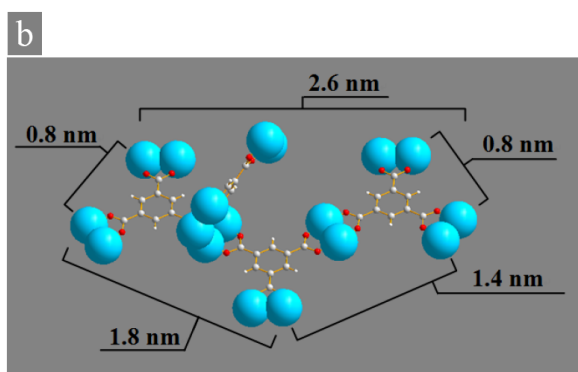
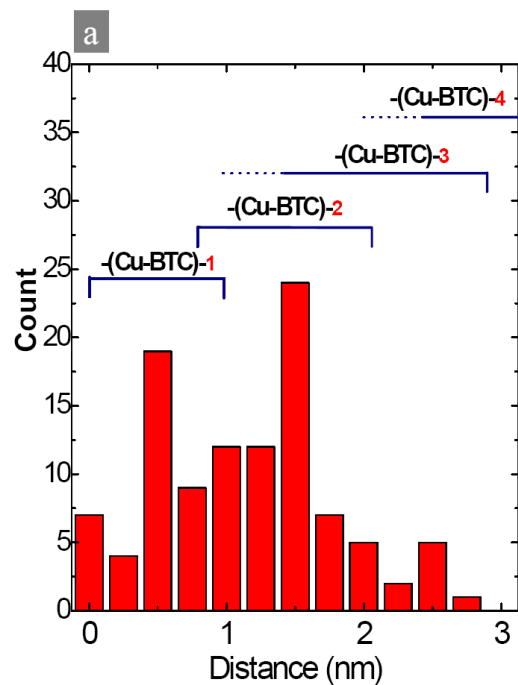


**Figure S24.** (a) The statistic of the intra-flake distance of the MOF nanocrystals. (b,c) Feature sizes of some typical  $-(\text{Cu-BTC})_{1-4}-$  fragments. (Atoms in blue: Cu(II), red: O, grey: C, light grey: H)

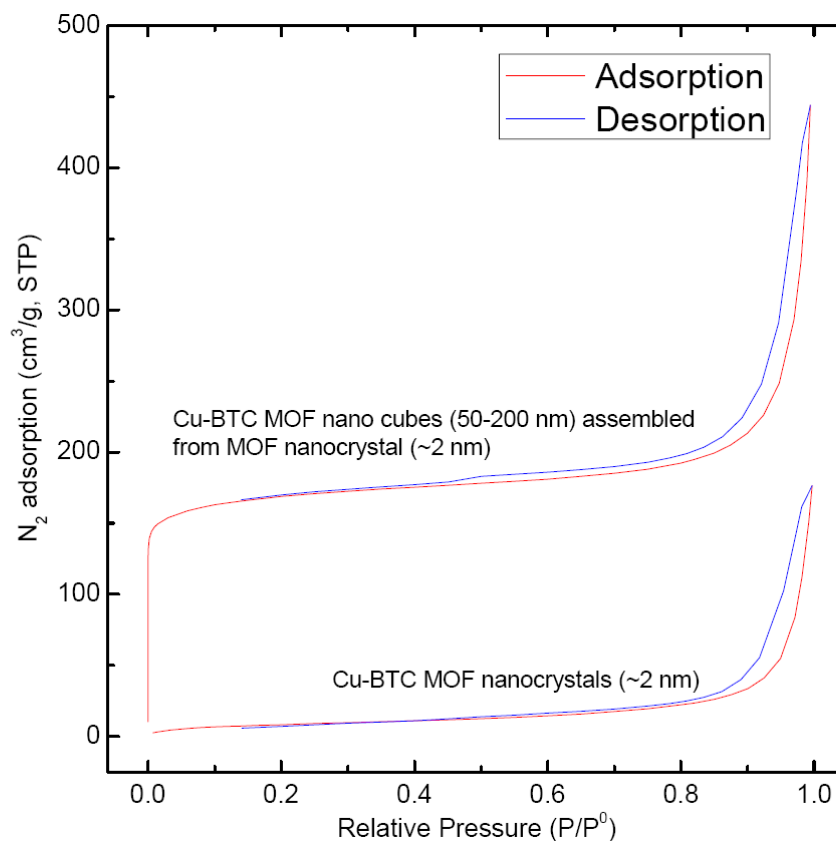


**Figure S25.** N<sub>2</sub> adsorption isotherms of Cu-BTC MOF nanocrystals (~2 nm) and assembled nano cubes measured at 77 K. Red line: adsorption; Blue line: desorption. The BET surface areas calculated from N<sub>2</sub> adsorption measurement are 31 and 571 m<sup>2</sup>/g, for the Cu-BTC MOF nanocrystals (~2 nm) and the assembled nano cubes, respectively. They both have an adsorption–desorption hysteresis loops between 0.8 to 1.0 relative pressure (P/P<sup>0</sup>), indicating the mesoporous structure [Ref. S11]. At low relative pressure (0 to 0.02), there is a sharp adsorption-saturation process of the MOF cubes just like typical MOF materials, suggesting the existence of micropores; while such adsorption is not found for the MOF nanocrystals. This is interpreted as the flexible ligands on the nanocrystal surface would block the pores of MOF nanocrystals. It hints that to enhance the BET value of those MOF nanocrystals in solid state, employing surface ligands with high rigidity could be one strategy. For both samples there is a sudden drop of the adsorption along the desorption branch in the P/P<sup>0</sup> about 0.45. This phenomenon is referred to the tensile strength effect [Ref. S12].

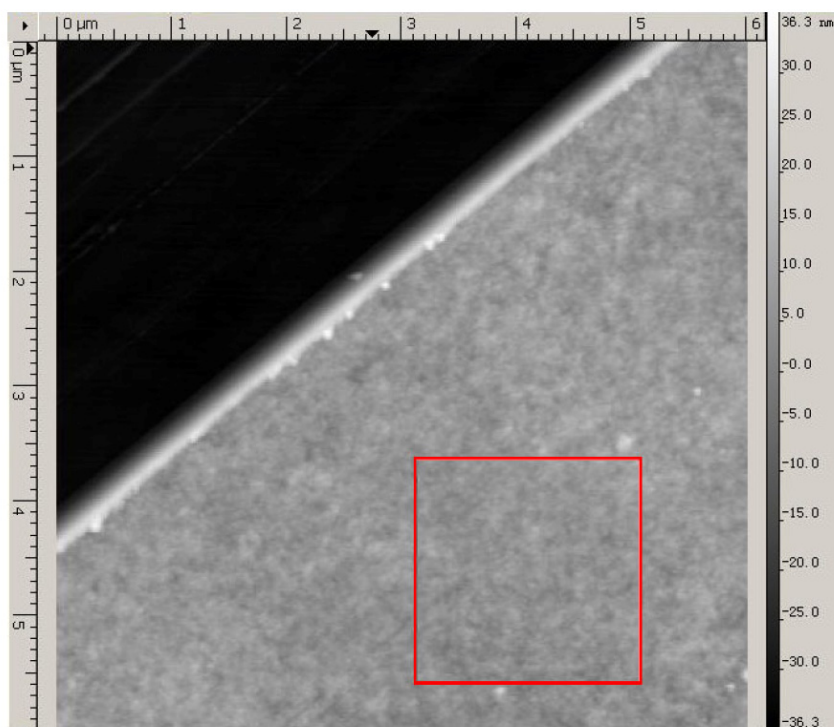


**Figure S26.** AFM image of the Cu-BTC MOF nanocrystal film. The statistical quantities in the red square are listed in [Table S2](#).

**Table S2.** The statistical quantities of the spin coated Cu-BTC MOF nanocrystal film in red square area in Fig. S28.

Width	1.93 $\mu\text{m}$
Height	1.93 $\mu\text{m}$
Ra	2.08 nm
Rms	2.62 nm
Rms (grain-wise)	2.62 nm
Skew	0.0201
Kurtosis	0.0893

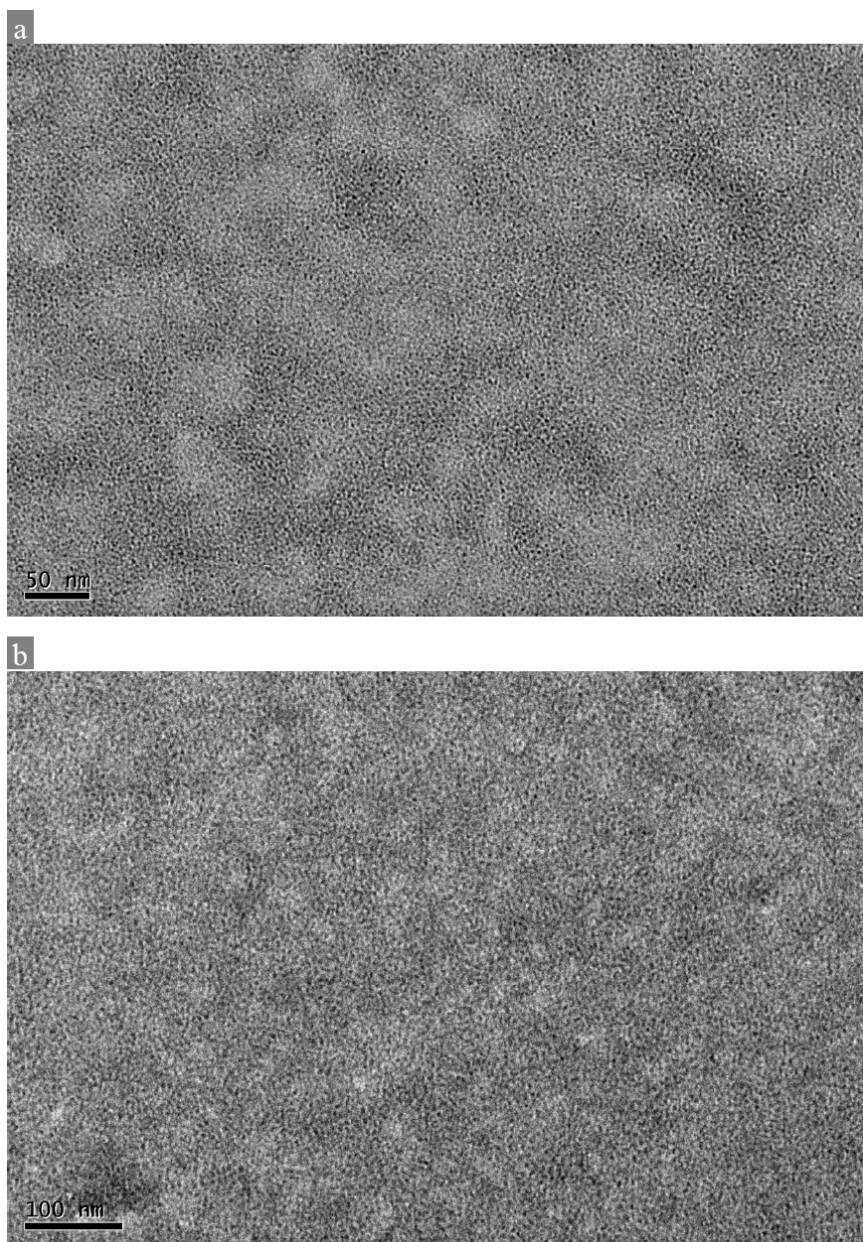


**Figure S27.** TEM images of multi-layers of Cu-BTC MOF nanocrystals on TEM grids. Cu-BTC nanocrystals synthesized by **(a)** using Cu(II)-caproate as precursor, and **(b)** using Cu(II)-oleate as precursor.

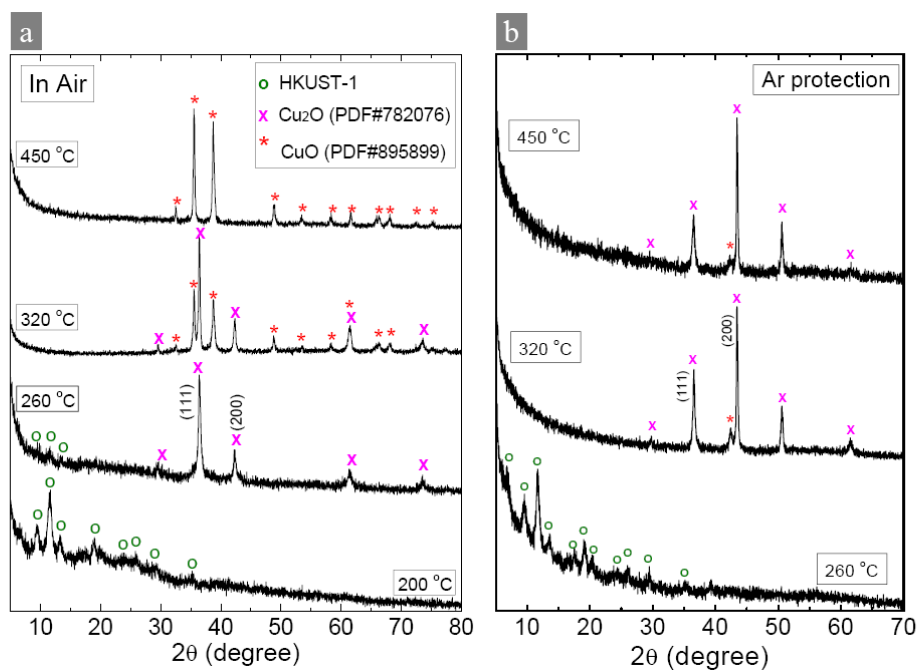


**Figure S28.** XRD patterns of the thermal treated Cu-BTC MOF nanocrystals (~2 nm). (a) Thermal treated in air at 200, 260, 320 and 450 °C in a muffle furnace, (b) with Ar protection at 260, 320 and 450 °C in a tubular furnace.

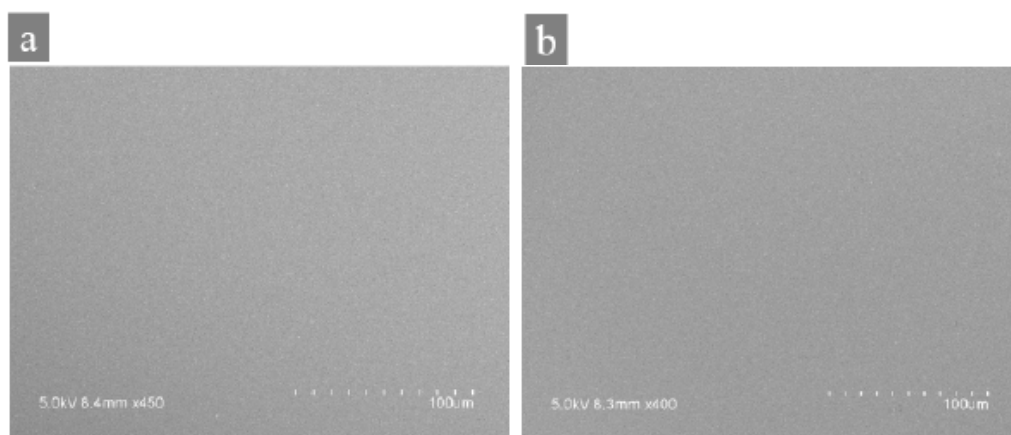


**Figure S29.** SEM images of spin-coated Cu-BTC MOF nanocrystal films (the  $\times 20$  sample) thermal treated in air at 260 °C (**a**) and 450 °C (**b**), forming smooth  $\text{Cu}_2\text{O}$  and  $\text{CuO}$  films, respectively. (scale bar: (**a**) (**b**)100  $\mu\text{m}$ ).

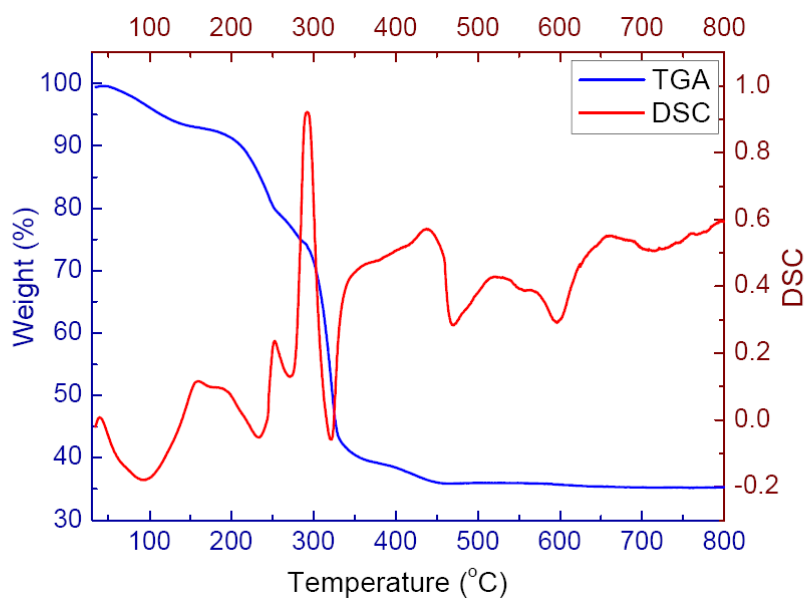


**Figure S30.** TGA/DSC of Cu-BTC MOF nanocrystals of  $\sim 2$  nm, measured from room temperature to 800 °C with a heating rate of 10 °C/min and N<sub>2</sub> protection. It shows that the MOF nanocrystals undergo a major endothermic peak at 290–300 °C, which correspond well with bulk HKUST-1 MOF crystals [Ref. S13, S14]. The MOF nanocrystals have additional weight loss steps and DSC peaks differing from that of the large MOF crystals. The  $\sim 5$  wt% loss of the MOF nanocrystals at 380–440 °C may be contributed by the oleic acid and/or oleylamine ligands (boiling points 360 and 364 °C respectively).

## References

- S1. Ameloot, R. *et al.* Direct patterning of oriented metal-organic framework crystals via control over crystallization kinetics in clear precursor solutions. *Adv. Mater.* **2010**, *22*, 2685.
- S2. Ghijsen, J. *et al.* Electronic structure of Cu<sub>2</sub>O and CuO. *Phys. Rev. B* **1988**, *38*, 11322.
- S3. Chen, H.; Wang, L. F.; Yang, J.; Yang, R. T. Investigation on hydrogenation of metal-organic frameworks HKUST-1, MIL-53, and ZIF-8 by hydrogen spillover. *J. Phys. Chem. C* **2013**, *117*, 7565.
- S4. Waechtler, T. *et al.* Copper oxide films grown by atomic layer deposition from bis(tri-n-butylphosphane)copper(I)acetylacetonate on Ta, TaN, Ru, and SiO<sub>2</sub>. *J. Electrochem. Soc.* **2009**, *156*, H453.
- S5. Chen, S. S. *et al.* Oxidation resistance of graphene-coated Cu and Cu/Ni alloy. *ACS Nano* **2011**, *5*, 1321.
- S6. Prestipino, C. *et al.* Local structure of framework Cu(II) in HKUST-1 metallorganic framework: Spectroscopic characterization upon activation and interaction with adsorbates. *Chem. Mater.* **2006**, *18*, 1337.
- S7. Xiao, B. *et al.* High-capacity hydrogen and nitric oxide adsorption and storage in a metal-organic framework. *J. Am. Chem. Soc.* **2007**, *129*, 1203.
- S8. Li, Y. W.; Yang, R. T. Hydrogen storage in metal-organic and covalent-organic frameworks by spillover. *AIChE J.* **2008**, *54*, 269.
- S9. Kalsin, A. M. *et al.* Electrostatic self-assembly of binary nanoparticle crystals with a diamond-like lattice. *Science* **2006**, *312*, 420.
- S10. Shevchenko, E. V.; Talapin, D. V.; Kotov, N. A.; O'Brien, S.; Murray, C. B. Structural diversity in binary nanoparticle superlattices. *Nature* **2006**, *439*, 55.
- S11. Groen, J. C.; Peffer, L. A. A.; Pérez-Ramírez, J. Pore size determination in modified micro- and mesoporous materials. Pitfalls and limitations in gas adsorption data analysis. *Micropor. Mesopor. Mat.* **2003**, *60*, 1.
- S12. Gregg, S. J.; Sing, K. S. W. *Adsorption Surface Area and Porosity*, second ed., p.154 (Academic Press, London, **1982**)
- S13. Schlichte, K.; Kratzke, T.; Kaskel, S. Improved synthesis, thermal stability and catalytic properties of the metal-organic framework compound Cu<sub>3</sub>(BTC)<sub>2</sub>. *Micropor. Mesopor. Mat.* **2004**, *73*, 81.
- S14. Lin, K. S.; Adhikari, A. K.; Ku, C. N.; Chiang, C. L.; Kuo, H. Synthesis and characterization of porous HKUST-1 metal organic frameworks for hydrogen storage. *Int. J. Hydrogen Energ.* **2012**, *37*, 13865.